



Tweaking the affinity of aryl-substituted diazosalicylato- and pyridine ligands towards Zn (II) and its neighbors in the periodic system of the elements, Cu (II) and Cd (II), and their antimicrobial activity

Tushar S. Basu Baul¹ | Khrawborlang Nongsiej¹ | Augustine Lamin Ka-Ot² | Santa Ram Joshi² | Irán Rojas León³ | Herbert Höpfl³

¹ Centre for Advanced Studies in Chemistry, North-Eastern Hill University, NEHU Permanent Campus, Umshing, Shillong 793 022, India

² Department of Biotechnology & Bioinformatics, North-Eastern Hill University, NEHU Permanent Campus, Umshing, Shillong 793 022, India

³ Centro de Investigaciones Químicas, Instituto de Investigación en Ciencias Básicas y Aplicadas, Universidad Autónoma del Estado de Morelos, Av. Universidad 1001, Cuernavaca 62209, Mexico

Correspondence

Tushar S. Basu Baul, Centre for Advanced Studies in Chemistry, North-Eastern Hill University, NEHU Permanent Campus, Umshing, Shillong 793 022, India.
Email: basubaulchem@gmail.com; basubaul@nehu.ac.in

Herbert Höpfl, Centro de Investigaciones Químicas, Instituto de Investigación en Ciencias Básicas y Aplicadas, Universidad Autónoma del Estado de Morelos, Av. Universidad 1001, Cuernavaca 62209, Mexico.
Email: hhopfl@uaem.mx

Funding information

Council of Scientific and Industrial Research, India, Grant/Award Number: 01 (2734)/13/ EMR-II, 2013 01 (2734)/13/ EMR-II; University Grants Commission, India, Grant/Award Number: 42-396/2013 (SR) 2013

A series of six new Zn (II) compounds, viz., [Zn(HL^{ASA})₂(Py)₂] (**1**), [Zn(HL^{MASA})₂(Py)₂] (**2**), [Zn(HL^{MASA})₂(4-MePy)₂] (**3**), [Zn(HL^{CASA})₂(4-MePy)₂] (**4**), [Zn(HL^{BASA})₂(Py)₂] (**5**), [Zn(HL^{BASA})₂(4-MePy)₂] (**6**) and representative Cu (II) and Cd (II) complexes, viz., [Cu(HL^{ASA})₂(Py)₂(H₂O)] (**7**) and [Cd(HL^{BASA})₂(Py)₃] (**8**) [(HL^{XASA})⁻ = *para*-substituted 5-[(*E*)-2-(aryl)-1-diazenyl]-2-hydroxybenzoate with X = H (ASA), Me (MASA), Cl (CASA) or Br (BASA); Py = pyridine; 4-MePy = 4-methylpyridine] have been synthesized and characterized by spectroscopic techniques and single-crystal X-ray diffraction analysis. The structural characterization of the compounds revealed distorted tetrahedral (**1–6**), square-pyramidal (**7**) and pentagonal-bipyramidal (**8**) coordination geometries around the metal atom, in which the aryl-substituted diazosalicylate ligands are coordinated only through the oxygen atoms of carboxylate groups, either in an anisobidentate or isobidentate mode; meanwhile, the 2-hydroxy groups of the monoanionic ligand (HL^{XASA})⁻ are involved only in intramolecular O-H...O hydrogen bonds with the carboxylate function. In the crystal structures of **1–8**, the complex molecules are assembled by π -stacking interactions giving mostly infinite 1D strands. The intermolecular binding in the solid state structures is accomplished by diverse additional non-covalent contacts including C-H...O, C-H...N, C-H... π , C-H...Br, O...Br, Br... π and van der Waals contacts. Although the primary and secondary ligands in the Zn (II) complex series **1–6** carry different substituents at the periphery (X = H, Me, Cl, Br for (HL^{XASA})⁻ and R = H, Me for 4-Py-R), five of the crystal structures were isostructural. Additionally, the antimicrobial activity of the proligands H₂L^{XASA} and their Zn (II), Cu (II) and Cd (II) compounds were studied in a comparative manner, showing high sensitivity (IZD \geq 20) against *Bacillus subtilis*.

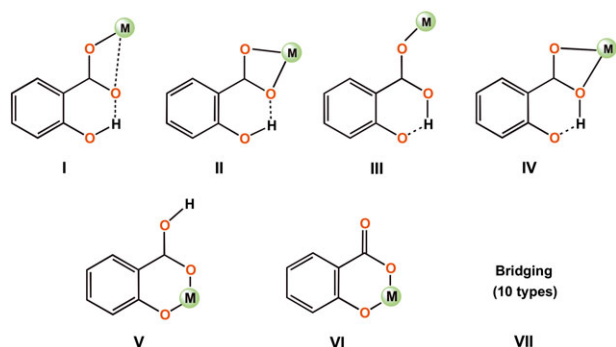
KEYWORDS

antimicrobial activity, diazo salicylate and pyridine ligands, SCXRD structure elucidation, zinc/copper/cadmium

1 | INTRODUCTION

Zinc is a biometal and an important constituent of various proteins.^[1] In its first coordination shell, zinc can incorporate ligands based on electronegative atoms such as nitrogen, oxygen and sulphur. The structural framework and physicochemical properties of zinc coordination compounds are dependent on the geometry and functionality of the ligands. Particularly, Zn (II) carboxylates have been widely studied and find applications as catalysts for carbon dioxide activation^[2] and C-C bond formation.^[3] Furthermore, zinc carboxylates derived from nitrogen donor ligands are an important class of compounds, which exhibit diverse coordination modes.^[4] Diprotic salicylic acid (H_2SA) and its derivatives are well-known non-steroidal anti-inflammatory, anti-pyretic and analgesic drugs^[5] with excellent affinity to transition metal ions.^[6] Transition metal complexes of salicylates in mono-anionic (HSA^-) and di-anionic (SA^{2-}) form are well known. In these complexes, the carboxylate group is generally deprotonated and can act as monodentate, bidentate or bridging moiety (Scheme 1).^[6] Although the COOH group in H_2SA is more acidic than the OH group, there are also reports on salicylate complexes, in which the carboxylate group is protonated and the hydroxyl group is deprotonated (Scheme 1; III-V).^[7-11]

On the other hand, linking H_2SA with a phenyldiazenyl group affords the diazenyl bridged pro-ligand 5-[(*E*)-2-(phenyl)-1-diazenyl]-2-hydroxybenzoic acid (here after H_2L^{ASA}) that has demonstrated antimicrobial, analgesic and antioxidant activity.^[12] Replacing the phenyl substituent by *para*-substituted aryl or pyridyl groups allows generating a large number of ligands, H_2L^{XASA} , which in combination with diverse secondary ligands have been used previously for complexation with Zn (II) ions, e.g., $[Zn(HL^{ASA})_2(3,5\text{-dimethylpyrazole})_2]$,^[13] $\{[Zn(HL^{PASA})_2(H_2O)_2] \cdot 2DMF\}_n$,^[14] $[Zn(HL^{ASA})_2(H_2O)_2] \cdot 2(2\text{-methylquinoline})$ ^[15] and



SCHEME 1 Coordination modes of (HSA^-) and (SA^{2-}) toward metal ions as characterized through single-crystal X-ray diffraction analysis

$[Zn_3(HL^{SASA})_2(Py)_2(H_2O)_8]_n$ ^[16] ($HL^{ASA} = 5\text{-}[(E)\text{-}2\text{-phenyl-1-diazenyl}]\text{-}2\text{-hydroxybenzoate}$, $HL^{PASA} = 5\text{-}[(E)\text{-}2\text{-}(4\text{-pyridyl})\text{-}1\text{-diazenyl}]\text{-}2\text{-hydroxybenzoate}$, $HL^{SASA} = 5\text{-}[(E)\text{-}2\text{-}(4\text{-sulphophenyl})\text{-}1\text{-diazenyl}]\text{-}2\text{-hydroxybenzoate}$). These complexes are mononuclear, but with the twofold functionalized pro-ligand 5-[(*E*)-2-(3-carboxy-4-hydroxyphenyl) diazen-1-yl]-2-hydroxybenzoic acid (H_4L^{ABisSA}) oligo- and polynuclear clusters are also known, which include $[Zn_4(HL^{ABisSA})_3(1,10\text{-phenanthroline})_2(H_2O)_2]_n$ with a rhombic tetrameric Zn_4O_4 core^[17] and $[Zn_6(L^{ABisSA})_3(4,4'\text{-bipyridine})_3(H_2O)_4] \cdot 4DMF$ with a Zn_6 -aggregate.^[18] The 1D coordination polymer $[Zn(H_2L^{ABisSA})(H_2O)_4]_n$ has a mononuclear ZnO_6 coordination environment.^[19] The coordination modes of the salicylate-fragments in these complexes fall within the options portrayed in Scheme 1 and the complexes display rich intra- and non-covalent intermolecular interactions including C-H...O, C-H...N and C-H... π contacts. Efforts were also made to link Zn (II) porphyrin complexes among each other by introducing a diazenyl-2-hydroxybenzoic acid fragment in the ligand where the diazenyl group serves as π -conjugated bridge and the carboxyl/hydroxyl groups as anchoring groups. These complexes demonstrated good photoelectric conversion efficiency in solar cells.^[20]

Recently, a variety of Zn (II) complexes with *N,O*-donor ligands containing a diazenyl group, i.e. 5-[(*E*)-2-(aryl)-1-diazenyl]quinolin-8-olate (L^{XAQ}) with X = Me, OMe, Et, OEt, NMe₂, Cl and Br, were investigated, in which the coordination environment of the zinc atom was modified by water molecules or other secondary ligands such as pyridine, 3-methylpyridine and 4-methylpyridine.^[21] The SCXRD structure analysis designated three variants of the Zn (II) coordination environment, i.e. $[Zn(L^{XAQ})_2(Py/3\text{-MePy}/4\text{-MePy})_2]$, $[Zn(L^{XAQ})_2(H_2O)_2]$ and $[Zn(L^{XAQ})_2(Py)]$, which had a significant influence on the supramolecular organization in the solid state.

Following our research interest to examine the molecular and crystal structures of Zn (II) compounds with aryldiazenyl-linked chelating ligands, the present work is focused on the preparation, characterization and structure elucidation of a series of Zn (II) compounds based on the aryldiazenyl linked *O,O*-chelating pro-ligands H_2L^{XASA} in combination with pyridine derivatives as ancillary ligands. The purpose of using pyridine derivatives is to enhance the solubility of the reaction constituents and to maintain the homogeneity of the reaction mixture, which is important for obtaining crystalline products. Additionally, pyridine can modulate the acidity of the metal center, which also influences the electronic properties of the chelators. To investigate the influence of other metals upon complexation with H_2L^{XASA} , coordination complexes of two metals adjacent to zinc in the periodic system of the elements were also examined,

namely Cu (one before Zn) and Cd (one below Zn). It is expected that the mixed ligand complexes can generate extended π -conjugated systems owing to the integration of the diazenyl chromophore, which can eventually act as electronic bank with potential applications for the design and tuning of the properties in optoelectronic materials.

The chemical structure of the six new Zn (II) compounds, viz., [Zn(HL^{XASA})₂(Py or 4-MePy)₂] (**1–6**) and two additional representative complexes [Cu (HL^{ASA})₂(Py)₂(H₂O)] (**7**) and [Cd (HL^{BASA})₂(Py)₃] (**8**) (HL^{XASA} = 5-[(*E*)-2-(aryl)-1-diazenyl]-2-hydroxybenzoate) are outlined in Scheme 2. The compounds were characterized by elemental analysis, IR, NMR, UV-vis spectroscopy and single crystal X-ray diffraction analysis. Finally, the *in vitro* antimicrobial activity of compounds **1–8** against three strains of bacteria and a fungal strain is reported.

2 | EXPERIMENTAL

2.1 | General considerations

Zn(OAc)₂·2H₂O, Cu(OAc)₂·H₂O (SD fine), Cd(OAc)₂·2H₂O (SRL), salicylic acid (Merck), *p*-toluidine, pyridine, 4-methylpyridine (Spectrochem), *p*-chloroaniline and *p*-bromoaniline (Himedia) were used without further purification, while aniline (SD Fine) was freshly distilled prior to use. The solvents used in the reactions were of AR grade and dried using standard procedures.

Melting points were measured using a Büchi melting point apparatus (M-560) and are uncorrected. IR spectra in the range 4000–400 cm⁻¹ were obtained on a Perkin Elmer Spectrum BX series FT-IR spectrophotometer with samples investigated as KBr discs. ¹H and ¹³C{¹H} NMR spectra, measured at 400.13 and 100.62 MHz, respectively, were recorded on a Bruker AMX 400 spectrometer. The ¹H and ¹³C chemical shifts were referenced to Me₄Si set at δ 0.00 ppm. Absorption measurements were carried out on a Perkin-Elmer Lambda25 spectrophotometer at ambient temperature in freshly prepared DMSO solutions.

For the *in vitro* antimicrobial assays, Mueller-Hinton agar (HiMedia) was used as nutrient liquid medium and standard antibiotic discs of chloramphenicol (C)³⁰ and fluconazole (FLC)²⁵ (HiMedia) were used as positive controls for bacteria and fungus, respectively.

2.2 | Synthesis of pro-ligands and their Zn (II), Cu (II) and Cd (II) compounds

The pro-ligands H₂L^{XASA}, viz., 5-[(*E*)-2-phenyl-1-diazenyl]-2-hydroxybenzoic acid (H₂L^{ASA}), 5-[(*E*)-2-(4-methylphenyl)-1-diazenyl]-2-hydroxybenzoic acid

(H₂L^{MASA}),^[22] 5-[(*E*)-2-(4-chlorophenyl)-1-diazenyl]-2-hydroxybenzoic acid (H₂L^{CASA})^[23] and 5-[(*E*)-2-(4-bromophenyl)-1-diazenyl]-2-hydroxybenzoic acid (H₂L^{BASA})^[22] were prepared starting from salicylic acid and the corresponding aniline using conventional diazonium salt chemistry, in accordance with literature procedures.

The method employed for the preparations of **1–8** are very similar; therefore, only the preparation of **1** is described in detail, as representative example. Yields of **1–8** have been reported relative to the respective metal acetates.

2.2.1 | Synthesis of [Zn(HL^{ASA})₂(Py)₂] (**1**)

Zn(OAc)₂·2H₂O (0.068 g, 0.31 mmol) in methanol (5 ml) was added drop-wise at room temperature to a stirred solution of H₂L^{ASA} (0.150 g, 0.62 mmol) in methanol (20 ml), which resulted in the immediate formation of a yellow-brown precipitate. The reaction mixture was heated to reflux for 3 hr and then filtered while hot. The residue was washed with hot methanol (3 x 5 ml) to remove undesired materials and dried *in vacuo*. The dried solid was dissolved in hot acetone (10 ml) containing pyridine (0.81 ml, 10.11 mmol) and filtered while hot. Slow evaporation of the filtrate afforded yellow crystals of **1**. Yield: 0.12 g (55%). M.p. 190–191°C. Found: C, 61.53; H, 3.82; N, 11.99%. Calcd. for C₃₆H₂₈N₆O₆Zn (MW = 706.02 gmol⁻¹): C, 61.24; H, 4.00; N, 11.90%. IR (cm⁻¹): 1623s, 1610s, 1569s, 1489s, 1451m, 1425m, 1384s, 1298m, 1261m, 1172w, 1072w, 836m, 770m, 687m, 574w, 524w. ¹H-NMR (DMSO-*d*₆); δ_{H} : 8.96–8.90 [m, 4H, ArH], 8.72 [s, 2H, ArH], 8.06–7.96 [m, 4H, ArH], 7.90–7.76 [m, 4H, ArH], 7.60–7.51 [m, 4H, ArH], 7.50–7.40 [m, 6H, ArH], 7.06 [d, 2H, ArH] ppm. The signal for the phenol group was not observed due to the presence of water in the solvent. ¹³C NMR (DMSO-*d*₆); δ_{C} : 175.5 [CO₂], 164.4 [C₂], 152.7, 149.5, 145.1, 140.2, 130.3, 129.0, 128.6, 127.3, 125.7, 122.6, 117.8, 116.4 [ArC] ppm.

2.2.2 | Synthesis of [Zn(HL^{MASA})₂(Py)₂] (**2**)

An analogous method to that used for the preparation of **1** was followed using Zn(OAc)₂·2H₂O (0.068 g, 0.31 mmol) and H₂L^{MASA} (0.158 g, 0.62 mmol). The dried solid was dissolved in hot acetone (10 ml) containing pyridine (0.81 ml, 10.11 mmol) and filtered while hot. Slow evaporation of the filtrate yielded yellow crystals of **2**. Yield: 0.14 g (61%). M.p. 203–205 °C. Found: C, 62.44; H, 4.48; N, 11.22%. Calcd. for C₃₈H₃₂N₆O₆Zn (MW = 734.08 gmol⁻¹): C, 62.17; H, 4.39; N, 11.45%. IR (cm⁻¹): 1623m, 1610s, 1567m, 1485s, 1451m, 1426m, 1380s, 1301m,

1259s, 1174m, 1071m, 1046w, 837s, 770m, 754m, 692s, 574m, 523w. $^1\text{H-NMR}$ ($\text{DMSO-}d_6$); δ_{H} : 12.8 [brs, 2H, OH], 8.90–8.80 [m, 4H, ArH], 8.62 [s, 2H, ArH], 7.96–7.82 [m, 4H, ArH], 7.82–7.70 [m, 4H, ArH], 7.25–7.10 [m, 4H, ArH], 7.00–6.90 [m, 4H, ArH], 7.06 [d, 2H, ArH], 2.33 [s, 6H, CH_3] ppm. $^{13}\text{C NMR}$ ($\text{DMSO-}d_6$); δ_{C} : 175.6 [CO_2], 164.2 [C2], 150.8, 149.5, 145.2, 140.7, 140.1, 129.7, 128.3, 127.2, 125.6, 122.5, 117.7, 116.4 [ArC], 21.5 [CH_3] ppm.

2.2.3 | Synthesis of $[\text{Zn}(\text{HL}^{\text{MASA}})_2(\text{4-MePy})_2]$ (3)

An analogous method to that used for the preparation of **1** was followed using $\text{Zn}(\text{OAc})_2 \cdot 2\text{H}_2\text{O}$ (0.068 g, 0.31 mmol) and $\text{H}_2\text{L}^{\text{MASA}}$ (0.158 g, 0.62 mmol). The dried solid was dissolved in hot acetone (10 ml) containing 4-methylpyridine (1.05 ml, 10.74 mmol) and filtered while hot. Slow evaporation of the filtrate yielded yellow crystals of **3**. Yield: 0.14 g (59%). M.p. 199–200 °C. Found: C, 63.43; H, 4.74; N, 11.01. Calcd. for $\text{C}_{40}\text{H}_{36}\text{N}_6\text{O}_6\text{Zn}$ (MW = 762.13 g mol^{-1}): C, 63.04; H, 4.76; N, 11.03%. IR (cm^{-1}): 1621s, 1591m, 1484m, 1430s, 1386m, 1362m, 1307w, 1259s, 1174w, 1071w, 836 s, 692w, 489w. $^1\text{H-NMR}$ ($\text{DMSO-}d_6$); δ_{H} : 12.8 [brs, 2H, OH], 8.72–8.58 [m, 6H, ArH], 7.95–7.87 [m, 2H, ArH], 7.76–7.66 [m, 4H, ArH], 7.30–7.18 [m, 8H, ArH], 7.00 [d, 2H, ArH], 2.35 and 2.32 [s, 12H, CH_3] ppm. $^{13}\text{C NMR}$ ($\text{DMSO-}d_6$); δ_{C} : 175.4 [CO_2], 164.2 [C2], 152.6, 150.8, 148.9, 145.2, 140.6, 129.7, 128.3, 127.1, 126.4, 122.5, 117.6, 116.6 [ArC], 21.5 and 21.4 [CH_3] ppm.

2.2.4 | Synthesis of $[\text{Zn}(\text{HL}^{\text{CASA}})_2(\text{4-MePy})_2]$ (4)

An analogous method to that used for the preparation of **1** was followed using $\text{Zn}(\text{OAc})_2 \cdot 2\text{H}_2\text{O}$ (0.068 g, 0.31 mmol) and $\text{H}_2\text{L}^{\text{CASA}}$ (0.171 g, 0.62 mmol). The dried solid was dissolved in hot acetone (10 ml) containing 4-methylpyridine (1.05 ml, 10.74 mmol) and filtered while hot. Slow evaporation of the filtrate yielded yellow crystals of **4**. Yield: 0.15 g (60%). M.p. 209–210 °C. Found: C, 57.05; H, 3.88; N, 10.40. Calcd. for $\text{C}_{38}\text{H}_{30}\text{Cl}_2\text{N}_6\text{O}_6\text{Zn}$ (MW = 802.97 g mol^{-1}): C, 56.84; H, 3.77; N, 10.47%. IR (cm^{-1}): 1622s, 1589m, 1574m, 1479m, 1432s, 1362m, 1306m, 1262s, 1172m, 1091m, 1072m, 1034w, 841s, 724m, 489w. $^1\text{H-NMR}$ ($\text{DMSO-}d_6$); δ_{H} : 13.0 [brs, 2H, OH], 8.76–8.70 [m, 6H, ArH], 8.05–7.93 [m, 2H, ArH], 7.85–7.80 [m, 4H, ArH], 7.46–7.40 [m, 4H, ArH], 7.42–7.38 [m, 4H, ArH], 7.06 [d, 2H, ArH], 2.44 [s, 6H, CH_3] ppm. $^{13}\text{C NMR}$ ($\text{DMSO-}d_6$); δ_{C} : 175.3 [CO_2], 164.7

[C2], 152.7, 151.1, 148.9, 144.9, 135.9, 129.2, 128.8, 127.7, 126.5, 123.8, 117.8, 116.7 [ArC], 21.5 [CH_3] ppm.

2.2.5 | Synthesis of $[\text{Zn}(\text{HL}^{\text{BASA}})_2(\text{Py})_2]$ (5)

An analogous method to that used for the preparation of **1** was followed using $\text{Zn}(\text{OAc})_2 \cdot 2\text{H}_2\text{O}$ (0.068 g, 0.31 mmol) and $\text{H}_2\text{L}^{\text{BASA}}$ (0.198 g, 0.62 mmol). The dried solid was dissolved in hot acetone (10 ml) containing pyridine (0.81 ml, 10.11 mmol) and filtered while hot. Slow evaporation of the filtrate yielded yellow crystals of **5**. Yield: 0.17 g (63%). M.p. 177–178 °C. Found: C, 50.02; H, 3.13; N, 10.04. Calcd. for $\text{C}_{36}\text{H}_{26}\text{Br}_2\text{N}_6\text{O}_6\text{Zn}$ (MW = 863.82 g mol^{-1}): C, 50.06; H, 3.03; N, 9.73%. IR (cm^{-1}): 1625s, 1607s, 1585s, 1573s, 1478s, 1428s, 1386s, 1306m, 1260m, 1172m, 1006w, 840s, 755w, 697m, 601m, 576m, 525w. $^1\text{H-NMR}$ ($\text{DMSO-}d_6$); δ_{H} : 13.1 [brs, 2H, OH], 8.90–8.78 [m, 4H, ArH], 8.70–8.63 [m, 2H, ArH], 8.05–7.90 [m, 4H, ArH], 7.87–7.80 [m, 4H, ArH], 7.60–7.50 [m, 4H, ArH], 7.50–7.40 [m, 4H, ArH], 7.02 [d, 2H, ArH] ppm. $^{13}\text{C NMR}$ ($\text{DMSO-}d_6$); δ_{C} : 174.4 [CO_2], 164.2 [C2], 150.4, 148.9, 144.2, 138.7, 135.3, 128.7, 128.0, 126.7, 124.7, 123.3, 117.2, 116.0 [ArC] ppm.

2.2.6 | Synthesis of $[\text{Zn}(\text{HL}^{\text{BASA}})_2(\text{4-MePy})_2]$ (6)

An analogous method to that used for the preparation of **1** was followed using $\text{Zn}(\text{OAc})_2 \cdot 2\text{H}_2\text{O}$ (0.068 g, 0.31 mmol) and $\text{H}_2\text{L}^{\text{BASA}}$ (0.198 g, 0.62 mmol). The dried solid was dissolved in hot acetone (10 ml) containing 4-methylpyridine (1.05 ml, 10.74 mmol) and filtered while hot. Slow evaporation of the filtrate yielded yellow crystals of **6**. Yield: 0.17 g (61%). M.p. 200–202 °C. Found: C, 51.20; H, 3.35; N, 9.36. Calcd. for $\text{C}_{38}\text{H}_{30}\text{Br}_2\text{N}_6\text{O}_6\text{Zn}$ (MW = 891.87 g mol^{-1}): C, 51.17; H, 3.39; N, 9.42%. IR (cm^{-1}): 1621s, 1477 m, 1456 m, 1430s, 1386 m, 1360 m, 1263 m, 1174 m, 1062 m, 841 s, 714w, 488w. $^1\text{H-NMR}$ ($\text{DMSO-}d_6$); δ_{H} : 12.9 [brs, 2H, OH], 8.70–8.55 [m, 6H, ArH], 8.95–7.85 [m, 2H, ArH], 7.75–7.65 [m, 4H, ArH], 7.40–7.20 [m, 8H, ArH], 7.96 [d, 2H, ArH], 2.37 [s, 6H, CH_3] ppm. $^{13}\text{C NMR}$ ($\text{DMSO-}d_6$); δ_{C} : 176.8 [CO_2], 166.1 [C2], 154.1, 152.5, 150.3, 146.4, 137.4, 130.6, 130.2, 128.6, 127.9, 125.2, 119.2, 118.1 [ArC], 23.0 [CH_3] ppm.

2.2.7 | Synthesis of $[\text{Cu}(\text{HL}^{\text{ASA}})_2(\text{Py})_2(\text{H}_2\text{O})]$ (7)

An analogous method to that used for the preparation of **1** was followed using $\text{Cu}(\text{OAc})_2 \cdot \text{H}_2\text{O}$ (0.061 g, 0.31 mmol) and $\text{H}_2\text{L}^{\text{ASA}}$ (0.150 g, 0.62 mmol). The dried solid was

dissolved in hot chloroform (10 ml) containing pyridine (0.81 ml, 10.11 mmol) and filtered while hot. Slow evaporation of the filtrate yielded dark green crystals of **7**. Yield: 0.14 g (63%). M.p. 174–175 °C. Found: C, 60.12; H, 4.25; N, 11.85. Calcd. for $C_{36}H_{30}CuN_6O_7$ (MW = 722.21 $g\ mol^{-1}$): C, 59.87; H, 4.19; N, 11.64%. IR (cm^{-1}): 1667w, 1607s, 1562s, 1487m, 1430s, 1382s, 1363s, 1301m, 1255s, 1151m, 843m, 797m, 688s, 508w.

2.2.8 | Synthesis of $[Cd(HL^{BASA})_2(Py)_3]$ (**8**)

An analogous method to that used for the preparation of **1** was followed using $Cd(OAc)_2 \cdot 2H_2O$ (0.082 g, 0.31 mmol) and H_2L^{BASA} (0.198 g, 0.62 mmol). The dried solid was dissolved in hot acetone (10 ml) containing pyridine (0.81 ml, 10.11 mmol) and filtered while hot. Slow evaporation of the filtrate yielded yellow crystals of **8**. Yield: 0.21 g (69%). M.p. 262 °C (dec.). Found: C, 49.70; H, 3.39; N, 9.92%. Calcd. for $C_{41}H_{31}Br_2CdN_7O_6$ (MW = 989.95 $g\ mol^{-1}$): C, 49.74; H, 3.16; N, 9.90%. IR (cm^{-1}): 1583s, 1464s, 1443s, 1388m, 1307m, 1216w, 1130w, 1070m, 1007w, 831s, 719w, 693m, 572w. 1H -NMR (DMSO- d_6); δ_H : 12.9 [brs, 2H, OH], 8.82–8.67 [m, 9H, ArH], 8.05–7.95 [m, 2H, ArH], 7.85–7.75 [m, 6H, ArH], 7.45–7.20 [m, 10H, ArH], 7.05 [d, 2H, ArH] ppm. ^{13}C NMR (DMSO- d_6); δ_C : 175.1 [CO₂], 164.2 [C2], 152.7, 150.8, 148.9, 145.7, 140.7, 129.7, 128.4, 127.1, 126.5, 122.5, 117.7, 116.6 [ArC] ppm.

2.2.9 | X-ray crystallography

Intensity data for compounds **1–8** were collected at ambient temperature with Mo- K_α radiation ($\lambda = 0.71073 \text{ \AA}$, monochromator: graphite) on an Agilent Technologies Xcalibur diffractometer equipped with an EOS CCD area detector. The measured intensities were reduced to F^2 and corrected for absorption using spherical harmonics (CryAlisPro).^[24] Intensities were corrected for Lorentz and polarization effects. Structure solution, refinement and data output were performed with the OLEX2 program package^[25] using SHELXT^[26] and SHELXL-2014.^[27] Non-hydrogen atoms were refined anisotropically. C-H and O-H hydrogen atoms were placed in geometrically calculated positions using the riding model. DIAMOND was used for the creation of figures.^[28]

The molecular structures of **1–4**, **6** and **7** exhibit crystallographic symmetry (2-axis), while the remaining compounds are asymmetric. The DELU instruction implemented in the SHELXL program was employed for the refinement of the slightly disordered $-N=N-C_6H_4-R$ fragments in **3–5**. In addition, in the refinement of compound **5** distance restraints were employed for the N=N

and C-N_{azenyli} bonds. Compound **7** crystallized in a chiral space group and refinement of the Flack parameter^[29] yielded the value 0.030(16), which confidently confirms that the refined model corresponds to the true enantiomorph. Crystallographic data for compounds **1–8** reported in this paper have been deposited with the Cambridge Crystallographic Data Centre (CCDC) as supplementary publication nos. CCDC-1887089-CCDC-1887096. These data can be obtained free of charge via www.ccdc.cam.ac.uk/getstructures.

2.3 | In vitro antimicrobial assay

The antimicrobial activity of pro-ligands HL^{XASA} (i.e. H_2L^{ASA} , H_2L^{MASA} , H_2L^{CASA} and H_2L^{BASA}) and the corresponding Zn (II), Cu (II) and Cd (II) compounds **1–8** was tested against three indicator bacterial strains, i.e., *Bacillus subtilis* MTCC 441, *Staphylococcus aureus* MTCC 96 and *Klebsiella pneumoniae* MTCC 109, and one fungal strain, *Candida albicans* MTCC 183, employing the agar well diffusion method.^[30] The stock solutions for pro-ligands HL^{XASA} and compounds **1–8** were prepared freshly in DMSO prior to use. The stock concentrations of the tested samples were $\sim 10,000 \mu g/ml$. Mueller-Hilton agar plates were swabbed with bacterial cell suspensions of the indicator bacterial strains adjusted to 1.5×10^8 colony forming units (CFU)/ml. Then, the agar surface was bored by using a sterilized cork borer to generate wells of 5 mm diameter, which were filled with a 100 μl aliquot of the corresponding test compound solution. A disc with the broad-spectrum antibiotic chloramphenicol (30 mcg) was used as positive control and a DMSO solution as negative control. Plates were incubated at 37 °C for 24 hr and the inhibition zones (mm) formed around the wells were measured using a Vernier caliper. For each organism, the experiments were conducted in triplicate and the antibacterial activity was evaluated by measuring the growth inhibition zone diameter (IZD, in mm). The activity was classified as high sensitivity for $IZD \geq 20$ mm, medium sensitivity for $IZD = 14–20$ mm, low sensitivity for $IZD = 7–13$ mm, and insignificant for $IZD < 7$ mm.

3 | RESULTS AND DISCUSSION

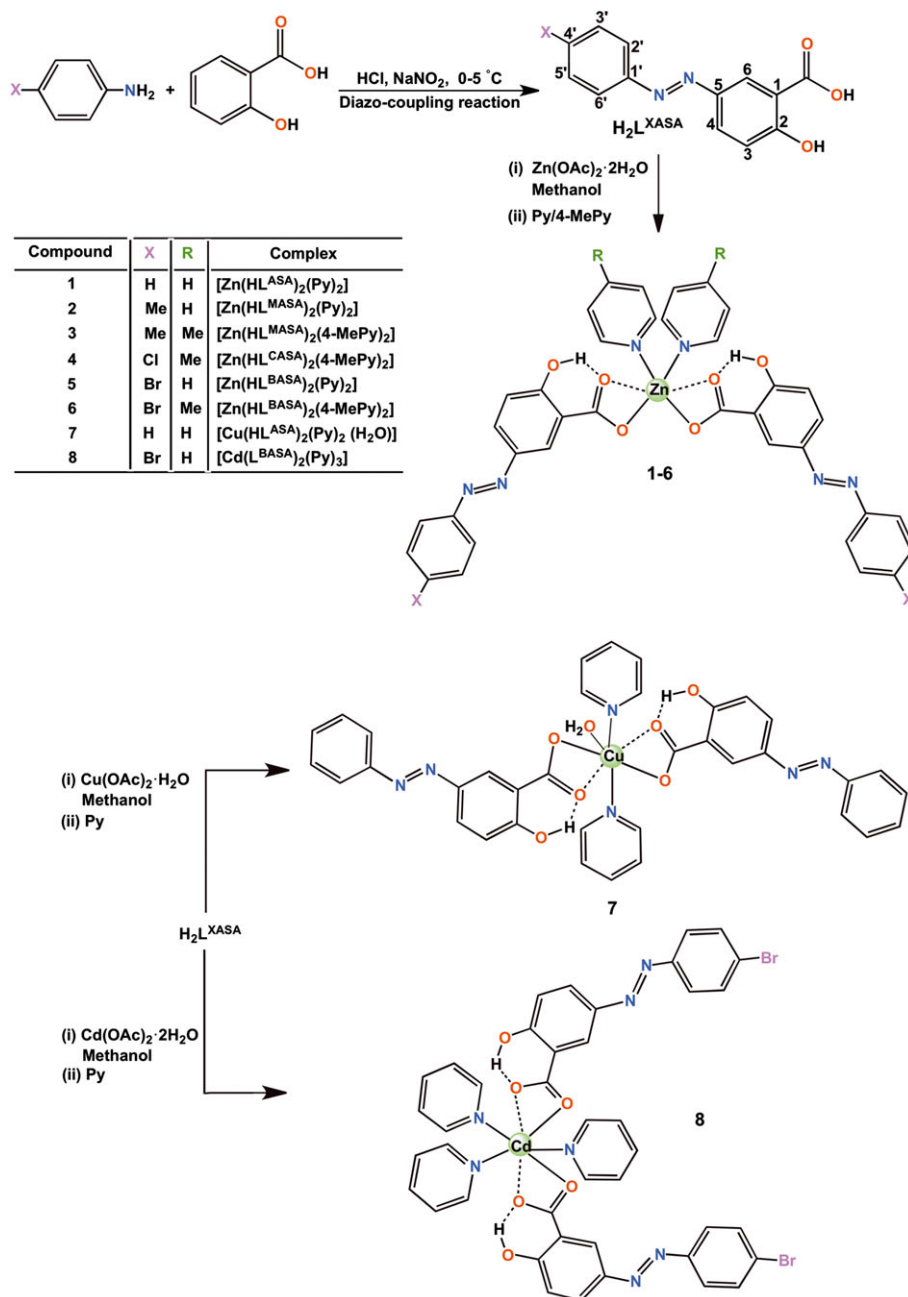
3.1 | Synthesis and spectroscopic characterization

The Zn (II) complexes **1–6** were prepared in methanol by reacting $Zn(OAc)_2 \cdot 2H_2O$ and H_2L^{XASA} in 1:2 molar ratio. Immediate formation of a precipitate was noticed and the precipitate was found to be soluble only in DMSO,

pyridine (Py) and pyridine derivatives such as methylpyridines (MePy). Crystallization experiments using an excess of Py or 4-MePy in acetone or chloroform afforded crystalline samples, in which either Py (**1**, **2** and **5**) or 4-MePy (**3**, **4** and **6**) was coordinated to the zinc atoms. The copper (II) and cadmium (II) complexes **7** and **8** were prepared analogously, however, in the case of **7** additionally a water molecule was incorporated in the coordination sphere of the copper atoms that possibly emerged from the starting reagent, $\text{Cu}(\text{OAc})_2 \cdot \text{H}_2\text{O}$ (Scheme 2). The products were obtained in moderate to good yield (>55%) in analytically pure form. Compounds **1–8** are colored crystalline solids that are fairly stable at

room temperature outside the mother liquor and melt or decompose above 170 °C.

The infrared spectra of compounds **1–8** are very similar and the most pertinent IR frequencies are included in the experimental section. The pro-ligands $\text{H}_2\text{L}^{\text{ASA}}$, $\text{H}_2\text{L}^{\text{MASA}}$, $\text{H}_2\text{L}^{\text{CASA}}$ and $\text{H}_2\text{L}^{\text{BASA}}$ display an intense IR absorption due to the asymmetric stretching vibration of the carboxyl group, $\nu_{\text{asym}}(\text{OCO})$, at 1664, 1658, 1666 and 1667 cm^{-1} , respectively, which is shifted to approximately 1620 cm^{-1} in the metal complexes (exception **7** and **8**), confirming that the carboxylate groups are bonded to the metal atoms. The IR spectra of **1–8** also displayed a band for $\nu_{\text{sym}}(\text{OCO})$ at around 1425 cm^{-1}



SCHEME 2 Synthesis and chemical structures of pro-ligands $\text{H}_2\text{L}^{\text{XASA}}$ and the Zn (II), Cu (II) and Cd (II) compounds **1–8**

with the frequency differences between ν_{asym} (OCO) and ν_{sym} (OCO) suggesting a monodentate coordination mode for the carboxylate ligands.^[31] The stretching vibration band typical for pyridine ligands, $\nu(\text{C-N})_{\text{py}}$, appear in the range 1485–1600 cm^{-1} , confirming the coordination of the pyridine nitrogen atom to the metal ions.^[32] The bonding hypotheses were subsequently confirmed by single-crystal X-ray diffraction studies (vide infra). Previously, the ^1H and ^{13}C NMR signals for pro-ligands $\text{H}_2\text{L}^{\text{XASA}}$ were assigned completely by the use of 2D ^1H - ^1H -correlation (COSY), heteronuclear single-quantum correlation (HSQC), constant time inverse-detection gradient accordion rescaled (CIGAR) and heteronuclear multiple-bond connectivity (HMBC) experiments.^[22] Compounds **1–8** were characterized by ^1H and ^{13}C NMR spectroscopy in CDCl_3 solutions (Figures S1–S14, ESI[†]). In general, compounds **1–6** and **8** exhibit broad ^1H NMR signals, which prevented the measurement of coupling constants. The signal assignments of the pro-ligands were subsequently extrapolated to the spectral analyses of the metal complexes (except **7**), owing to the data similarity. Aside from the signals for metal-coordinated $(\text{HL}^{\text{XASA}})^-$, the ^1H and $^{13}\text{C}\{^1\text{H}\}$ NMR spectra of **1–6** and **8** displayed also the expected signals for the secondary Py/4-MePy ligands. The UV–Vis absorption spectra of $\text{H}_2\text{L}^{\text{XASA}}$, and the corresponding Zn (II), Cu (II) and Cd (II) compounds **1–8** in DMSO are depicted in Figure S15, ESI[†]. Table S1 summarizes the most relevant characteristics of the UV–Vis data, showing similar absorption spectra of **1–8** with slight changes in the absorption maximum. The compounds were found to be non-emissive in DMSO solution.

3.2 | Description of the X-ray crystal structures

Crystals of compounds **1–8** suitable for single-crystal X-ray diffraction (SCXRD) analysis were obtained by slow evaporation of solutions of the respective compounds in acetone/pyridine (**1**, **2**, **5** and **8**), acetone/4-methylpyridine (**3**, **4** and **6**) and chloroform/pyridine (**7**). Crystal data, data collection parameters and convergence results are listed in Table 1. The asymmetric units of the crystal structures including displacement ellipsoids are shown in Figures S16–S23, ESI[†].

Despite the variation of the substituents in the primary and secondary ligands (Scheme 2, Figures 1–6), five of the six Zn (II) complexes **1–6** are isostructural, as indicated by the unit cell parameters given in Table 1 and the common monoclinic space group ($C2/c$). Only compound **5** crystallized in the monoclinic space group $P2_1/n$. As a result, the molecular and crystal structures of compounds **1–4** and **6**

are closely related. In these compounds, the zinc atoms are embedded in ZnN_2O_2 polyhedra exhibiting a crystallographic 2-axis. The metal coordination spheres are constituted by the oxygen atoms from the carboxylate groups of two mono anionic $(\text{HL}^{\text{XASA}})^-$ ligands bound in mode I as shown in Scheme 1 and the nitrogen atoms from two pyridine ligand molecules. The coordination geometries are significantly distorted from ideal values for a tetrahedron, due to two weak secondary $\text{Zn}\cdots\text{O}_{\text{OCO}}$ interactions, thus generating an overall bicapped tetrahedral environment (Figures 1–4, 6). The distortion is illustrated by comparison of the $\text{O}_{\text{OCO}}\text{-Zn-N}_{\text{py}}$ bond angles with values in the range of 101.0(2)–101.60(10) $^\circ$ and 124.22(8)–129.35(11) $^\circ$ (Table 2). The secondary $\text{O}_{\text{OCO}}\cdots\text{Zn}$ interactions are localized between the atoms forming the larger $\text{O}_{\text{OCO}}\text{-Zn-N}_{\text{py}}$ bond angles. The $\text{O}_{\text{OCO}}\cdots\text{Zn}$ contacts can be considered as weak interactions, since the distances in the range of 2.688(3)–2.865(2) Å approach the sum of the van der Waals radii of oxygen and zinc (2.91 Å). As a consequence, the remaining bond angles in the coordination polyhedra are significantly smaller than the ideal value of 109.5 $^\circ$ and decrease in all cases (except compound **1**) in the order $\text{N}_{\text{py}}\text{-Zn-N}_{\text{py}}$ [102.5(3)–106.69(13) $^\circ$] > $\text{O}_{\text{OCO}}\text{-Zn-N}_{\text{py}}$ [101.0(2)–101.60(10) $^\circ$] > $\text{O}_{\text{OCO}}\text{-Zn-O}_{\text{OCO}}$ [96.09(16)–99.76(12) $^\circ$; 103.37(10) $^\circ$ for **1**] (Table 2). The Zn– O_{OCO} and Zn– N_{py} bond distances of the ZnN_2O_2 core are 1.9488(17)–2.011(5) Å and 2.0275(19)–2.048(3) Å, respectively. Similar values were observed in related Zn (II) complexes of composition $[\text{Zn}(\text{OOCR})_2(\text{Py}^{\text{X}})_2]$, e.g., bis(4-(dimethylamino)pyridine- κN)-bis(2-hydroxybenzoato- κO)-zinc (II),^[33] bis(3-hydroxypyridine- κN)-bis(3-nitrobenzoato- κO)-zinc (II)^[34] and bis(2-fluorobenzoato- κO)-bis(pyridin-2-amine- κN^1)-zinc (II).^[35]

Although the constitution of the coordination sphere in compound **5** is identical to that found for **1–4** and **6** (ZnN_2O_2 core with two secondary $\text{O}\cdots\text{Zn}$ interactions), there are significant differences in the molecular conformation and the supramolecular organization (Figure 7). In **1–4** and **6**, the faces capped by the weakly bound oxygen atoms are the triangles formed by the two N_{py} nitrogen atoms and one of the O_{OCO} oxygen atoms (O1/O1^i), giving $\text{O}\cdots\text{Zn}\cdots\text{O}$ bond angles approaching 180 $^\circ$ [173.58(8)–179.6(1) $^\circ$]; meanwhile, in **5** the secondary bonding occurs via the $\text{O}_{\text{OCO}}\text{-O}_{\text{OCO}}\text{-N}_{\text{py}}$ faces with a $\text{O}\cdots\text{Zn}\cdots\text{O}$ bond angle of 83.4(1) $^\circ$. As a consequence, in the molecular structure of **5** the $\text{O}_{\text{OCO}}\text{-Zn-O}_{\text{OCO}}$ bond angle is significantly enlarged [128.41(14) $^\circ$] when compared to the remaining zinc complexes [96.09(16)–103.37(10) $^\circ$] and the $\text{O}_{\text{OCO}}\text{-Zn-N}_{\text{py}}$ bond angles are now in the range of 100.27(15)–110.76(15) $^\circ$. Nevertheless, the $\text{N}_{\text{py}}\text{-Zn-N}_{\text{py}}$ bond angles are rather constant for all six complexes [102.5(3)–106.69(13) $^\circ$] (Table 2).

Another common aspect of all Zn (II) complexes (**1–6**) is the presence of an intramolecular $\text{O-H}\cdots\text{O}$ hydrogen bond

TABLE 1 Crystal data, data collection parameters and convergence results for compounds 1–8

	1	2	3	4	5	6	7	8	
CCDC No.	1887093	1887091	1887089	1887090	1887092	1887095	1887094	1887096	
Empirical formula	C ₃₆ H ₂₈ N ₆ O ₆ Zn	C ₃₈ H ₃₂ N ₆ O ₆ Zn	C ₄₀ H ₃₆ N ₆ O ₆ Zn	C ₃₈ H ₃₀ Cl ₂ N ₆ O ₆ Zn	C ₃₆ H ₂₆ Br ₂ N ₆ O ₆ Zn	C ₃₈ H ₃₀ Br ₂ N ₆ O ₆ Zn	C ₃₆ H ₃₀ CuN ₆ O ₇	C ₄₁ H ₃₁ Br ₂ CdN ₇ O ₆	
Formula weight	706.01	734.06	762.12	802.95	863.82	891.87	722.20	989.95	
Temperature (K)	293	295	293	295	294	294	293	295	
Crystal system	Monoclinic	Monoclinic	Monoclinic	Monoclinic	Triclinic	Monoclinic	Orthorhombic	Monoclinic	
Space group	C2/c	C2/c	C2/c	C2/c	P-1	C2/c	P2 ₁ 2 ₁ 2	P2 ₁ /n	
<i>a</i> (Å)	33.992(7)	33.809(3)	32.601(3)	31.906(3)	9.4257(8)	32.256(5)	9.9646(9)	9.0289(5)	
<i>b</i> (Å)	5.8856(7)	6.0352(4)	6.4023(7)	6.4131(7)	12.8197(12)	6.1881(8)	28.0228(17)	10.8636(8)	
<i>c</i> (Å)	16.860(4)	17.246(2)	17.9940(15)	18.3357(14)	16.0450(14)	18.541(3)	6.0189(4)	41.131(2)	
α (°)	90	90	90	90	111.175(8)	90	90	90	
β (°)	107.550(18)	97.273(9)	97.095(8)	96.308(7)	103.266(7)	91.300(12)	90	93.853(5)	
γ (°)	90	90	90	90	90.962(7)	90	90	90	
Volume (Å ³)	3216.1(11)	3490.5(6)	3727.0(7)	3729.1(6)	1749.0(3)	3699.8(9)	1680.7(2)	4025.3(4)	
<i>Z</i>	4	4	4	4	2	4	2	4	
ρ_{calc} (g/cm ³)	1.458	1.397	1.358	1.430	1.640	1.601	1.427	1.634	
μ (mm ⁻¹)	0.821	0.760	0.714	0.856	3.042	2.879	0.709	2.584	
F(000)	1456.0	1520	1584	1648	864	1792	746	1968	
Crystal size (mm ³)	0.21 × 0.21 × 0.23	0.08 × 0.15 × 0.20	0.02 × 0.22 × 0.33	0.14 × 0.16 × 0.16	0.15 × 0.18 × 0.35	0.12 × 0.25 × 0.29	0.15 × 0.23 × 0.29	0.12 × 0.17 × 0.26	
2 θ range for data collection (°)	7.04–58.20	6.86–58.28	6.49–57.87	6.81–57.81	6.29–58.03	6.77–57.87	6.92–58.32	6.10–58.11	
Index ranges	–46 ≤ <i>h</i> ≤ 23 –7 ≤ <i>k</i> ≤ 7 –21 ≤ <i>l</i> ≤ 22	–44 ≤ <i>h</i> ≤ 44 –4 ≤ <i>k</i> ≤ 8 –23 ≤ <i>l</i> ≤ 9	–38 ≤ <i>h</i> ≤ 40 –8 ≤ <i>k</i> ≤ 4 –24 ≤ <i>l</i> ≤ 23	–39 ≤ <i>h</i> ≤ 35 –4 ≤ <i>k</i> ≤ 7 –14 ≤ <i>l</i> ≤ 24	–11 ≤ <i>h</i> ≤ 12 –16 ≤ <i>k</i> ≤ 17 –21 ≤ <i>l</i> ≤ 15	–35 ≤ <i>h</i> ≤ 43 –8 ≤ <i>k</i> ≤ 7 –22 ≤ <i>l</i> ≤ 24	–8 ≤ <i>h</i> ≤ 13 –37 ≤ <i>k</i> ≤ 21 –6 ≤ <i>l</i> ≤ 8	–12 ≤ <i>h</i> ≤ 7 –13 ≤ <i>k</i> ≤ 13 –30 ≤ <i>l</i> ≤ 52	
Reflections collected	6382	6872	7167	7166	12184	13168	4843	16821	
Independent reflections [<i>R</i> _{int}]	3693 [0.027]	4032 [0.027]	4244 [0.033]	4175 [0.027]	7813 [0.039]	4404 [0.072]	3487 [0.029]	9196 [0.041]	

(Continues)

TABLE 1 (Continued)

	1	2	3	4	5	6	7	8
Data/restraints/ parameters	3693/0/223	4032/0/233	4244/36/243	4175/36/242	7813/0/462	4404/39/242	3487/0/229	9196/0/516
Goodness-of-fit on F^2	1.019	1.039	1.044	1.041	1.034	1.012	1.109	1.124
R_1 [$I \geq 2\sigma(I)$]	0.0451	0.0535	0.0580	0.0598	0.0656	0.0909	0.0463	0.0588
wR_2 [all data]	0.1164	0.1384	0.1493	0.1572	0.1105	0.2054	0.1166	0.1082
Diff. peak/hole ($e \text{ \AA}^{-3}$)	-0.50/0.33	-0.32/0.54	-0.31/0.61	-0.35/0.64	-0.60/-0.61	-0.62/1.15	-0.53/0.42	-0.65/0.78

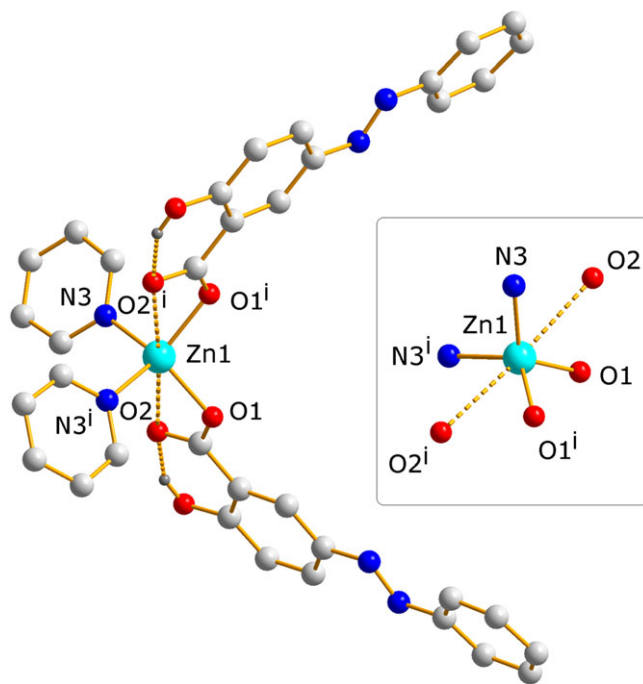


FIGURE 1 Perspective view of the molecular structure of compound 1 with partial atom labeling scheme. Symmetry operator: (i) 1-x, y, 0.5-z. For clarity, most of the hydrogen atoms are omitted

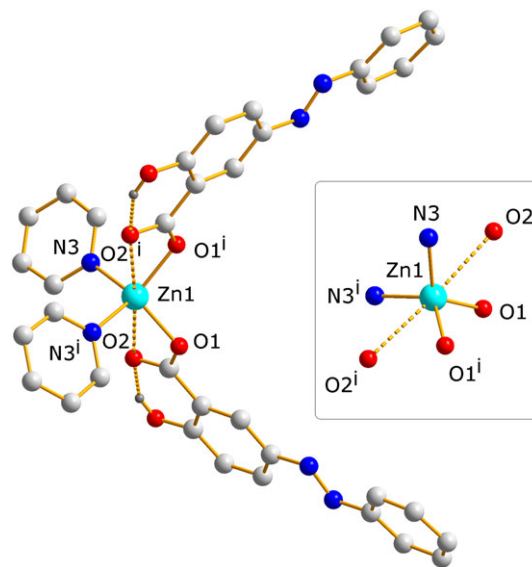


FIGURE 2 Perspective view of the molecular structure of compound 2 with partial atom labeling scheme. Symmetry operator: (i) 1-x, y, 0.5-z. For clarity, most of the hydrogen atoms are omitted

in the $(HL^{XASA})^-$ ligand with $H \cdots O$ and $O \cdots O$ distances in the range of 1.78–1.83 Å and 2.511(3)–2.551(6) Å, respectively. The $O-H \cdots O$ angles vary from 145 to 148° (Table S2).

Contrary to the Zn (II) complexes 1–6, the Cu (II) and Cd (II) analogues adopt higher coordination numbers by incorporating additional solvent/base molecules in the

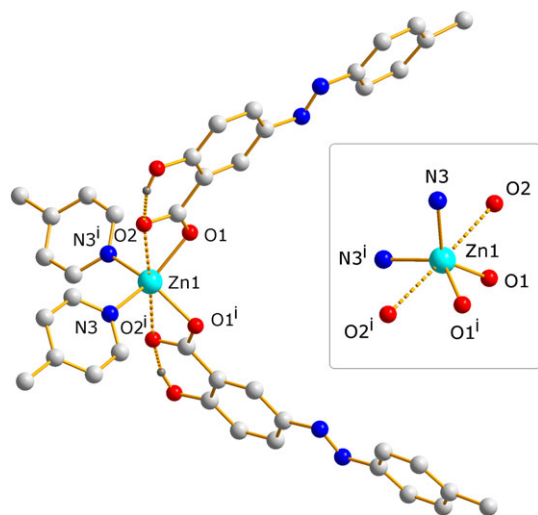


FIGURE 3 Perspective view of the molecular structure of compound **3** with partial atom labeling scheme. Symmetry operator: (i) 1-x, y, 1.5-z. For clarity, most of the hydrogen atoms are omitted

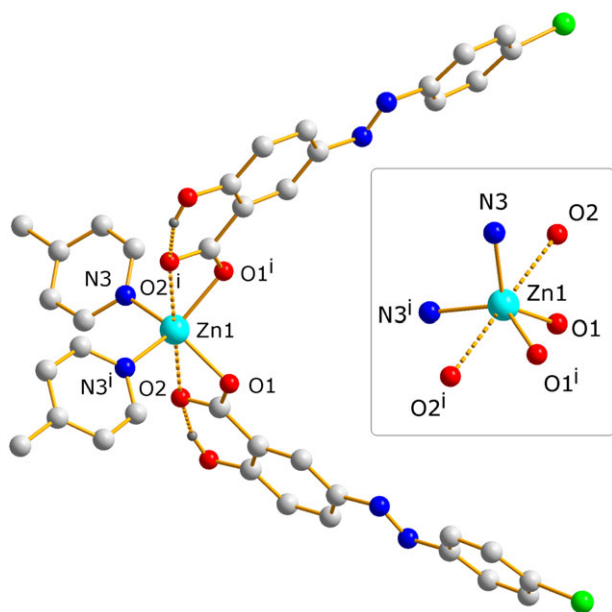


FIGURE 4 Perspective view of the molecular structure of compound **4** with partial atom labeling scheme. Symmetry operator: (i) 1-x, y, 1.5-z. For clarity, most of the hydrogen atoms are omitted

coordination sphere. The five-coordinate Cu (II) complex **7** comprises a symmetric (crystallographic 2-axis) CuN_2O_3 polyhedron with distorted square-pyramidal geometry formed by two $(\text{HL}^{\text{ASA}})^-$, two pyridine and one water ligand molecules (Figure 8). The basal plane is constituted by *trans*-oriented pairs of $(\text{HL}^{\text{ASA}})^-$ and pyridine ligands with $\text{O}_{\text{OCO}}\text{-Cu-O}_{\text{OCO}}$ and $\text{N}_{\text{py}}\text{-Cu-N}_{\text{py}}$ bond angles of $174.0(2)$ and $176.0(2)^\circ$, respectively. Accordingly, the bond angles of the *cis*-oriented donor atoms in the basal plane

approach 90° [$\text{N}_{\text{py}}\text{-Cu-O}_{\text{OCO}} = 89.32(13)$ and $90.47(13)^\circ$]; meanwhile, the apical position is occupied by the water ligand, which is, as expected, weaker bound than the anionic ligands [$\text{Cu-O}_{\text{w}} = 2.214(4) \text{ \AA} \leftrightarrow \text{Cu-O}_{\text{OCO}} = 1.973(3) \text{ \AA}$]. The $\text{O}_{\text{w}}\text{-Cu-O}_{\text{OCO}}/\text{N}_{\text{py}}$ bond angles approach 90° (Table 3), indicating only a small deviation of the metal ion from the basal plane, which is attributed to two weak secondary $\text{O}_{\text{OCO}}\cdots\text{Cu}$ interactions of the carboxylate groups of $(\text{HL}^{\text{ASA}})^-$ with the Cu (II) ions (binding mode I, Scheme 1). Although the $\text{O}_{\text{OCO}}\cdots\text{Cu}$ distance of $3.014(4) \text{ \AA}$ exceeds the sum of the van der Waals radii of the atoms involved (2.92 \AA), the close proximity of the metal ion to the mean plane of the square pyramid base (0.09 \AA) is indicative of an attractive interaction. Complexes of similar composition, $[\text{Cu}(\text{OOCR})_2(\text{Py}^{\text{X}})_2(\text{H}_2\text{O})]$, were reported previously by the research groups of Smith ($\text{R} = -\text{CH}_2\text{O}(2\text{-FC}_6\text{H}_4)$ and $-\text{CH}_2\text{O}(2\text{-Me}, 4\text{-ClC}_6\text{H}_3)$; $\text{X} = \text{H}$)^[36,37] and Valach ($\text{R} = \text{Me}$; $\text{X} = \text{NH}_2$).^[38]

Cd (II) ions are significantly larger than Zn (II) and Cu (II) ions, which explains the seven-fold coordination found in compound **8**. As can be seen from Figure 9, the pentagonal-bipyramidal coordination polyhedron in **8** is comprised of a CdN_3O_4 core, in which contrary to compounds **1–7**, the carboxylate groups approach an isobidentate coordination mode (binding mode II, Scheme 1), as can be realized from the corresponding Cd-O- O_{OCO} distances [$\text{Cd-O1/O2} = 2.406(3)/2.464(4) \text{ \AA}$ and $\text{Cd-O4/O5} = 2.349(3)/2.560(3) \text{ \AA}$] (Table 4). The oxygen atoms and one of the pyridine ligands (N7) comprise the pentagonal plane of the coordination sphere with $\text{O}_{\text{OCO}}\text{-Cd-O}_{\text{OCO}}/\text{N}_{\text{py}}$ bond angles in the range of $53.24(10)$ – $87.31(12)^\circ$ between neighboring donor atoms. The deviation from the ideal value of 72° is due to the formation of two four-membered chelate rings with the O_{OCO} oxygen atoms. Distortion from the ideal polyhedron is also reflected from the $\text{N}_{\text{py}}\text{-Cd-N}_{\text{py}}$ angle of $166.00(14)^\circ$ formed between the pyridine ligands occupying the axial sites (N3 and N6). The Cd- N_{py} distances in the range of $2.325(4)$ – $2.361(4) \text{ \AA}$ are as expected, as observed from the geometric data reported previously for structurally related Cd (II) dicarboxylates containing pyridine in the coordination sphere.^[39–41] As for **1–6**, the molecular structures of **7** and **8** are stabilized by intramolecular O-H \cdots O hydrogen bonds (Table S2).

3.3 | Description of the supramolecular structures of 1–8

3.3.1 | Analysis of the Zn (II) compounds 1–6

As mentioned in the introduction, π -stacking interactions are relevant for the electron transport and optical

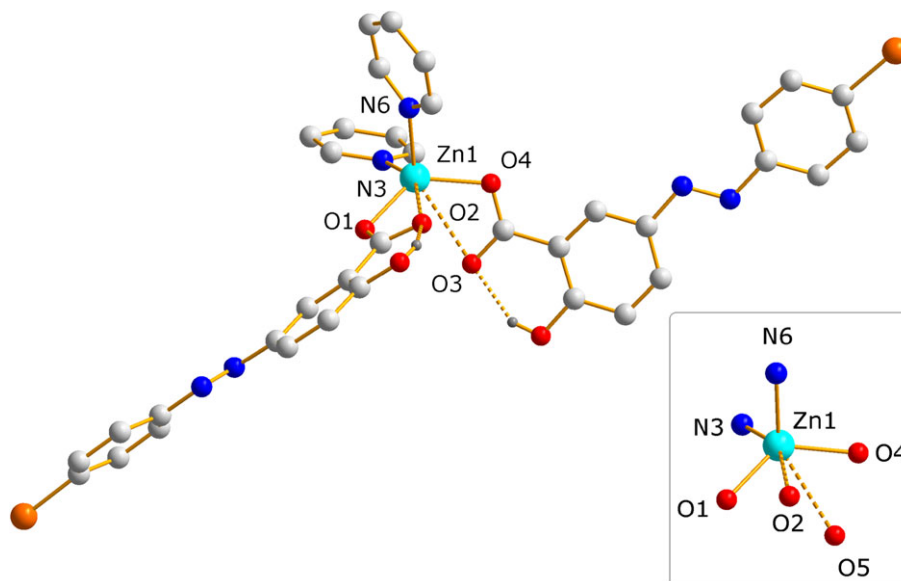


FIGURE 5 Perspective view of the molecular structure of compound **5** with partial atom labeling scheme. For clarity, most of the hydrogen atoms are omitted

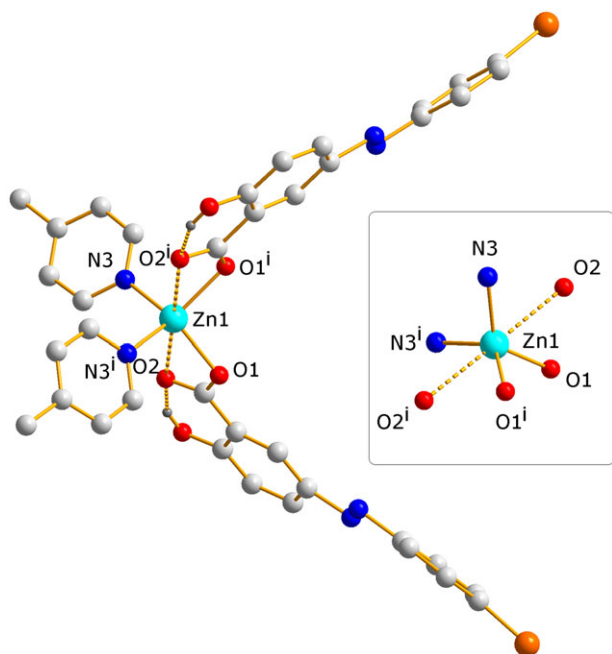


FIGURE 6 Perspective view of the molecular structure of compound **6** with partial atom labeling scheme. Symmetry operator: (i) 1-x, y, 1.5-z. For clarity, most of the hydrogen atoms are omitted

properties of metal complexes derived from diazenyl ligands.^[20,21] In view of these characteristics and with the purpose to analyze the influence of the substituents at the periphery of the $(\text{HL}^{\text{XASA}})^-$ ligands and the pyridine coordination to the Zn (II) centers, the supramolecular interactions in the crystal structures of **1–6** were examined. As expected from the similar unit cell parameters for compounds **1–4** and **6**, the overall supramolecular

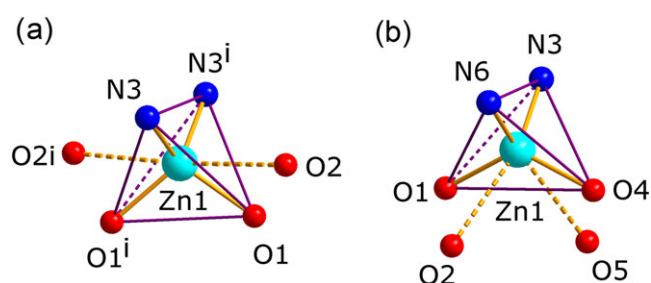
organization is closely related, albeit there are some differences in the specific intermolecular interactions. The supramolecular organization of these complexes is dominated by π -interactions, giving 1D π -stacked assemblies along the [0 1 0] direction. This arrangement is facilitated by the double-V shaped conformation of the molecular structures that orients the terminal $-\text{C}_6\text{H}_4\text{X}$ groups in *syn*-orientation (Figure 1–4, 6) and enables π -interactions between the terminal $-\text{C}_6\text{H}_4\text{X}$ moieties and the salicylate rings of adjacent metal-coordinated ligands. The intermolecular binding in the 1D strands is further strengthened by C-H \cdots O contacts formed between the pyridine ligands and the salicylate moieties. As representative example, Figure 10 shows the assembly found in the crystal structure of **1**. The centroid \cdots centroid distance of the π -interactions in **1** is 3.97 Å and ranges from 3.84–4.39 Å for **2**, **3**, **4** and **6**. Within the crystal structure of **1**, adjacent π -stacks run in opposite directions and are connected further through additional C-H \cdots O hydrogen bonds, relatively weak π -interactions between adjacent pyridine ligands (centroid \cdots centroid, 4.75 Å) and van der Waals contacts (Table S3). In **2**, **3**, **4** and **6**, the primary and the secondary ligands are involved in additional interactions of the $\pi\cdots\pi$ (**2**, **3**, **4** and **6**), C-H $\cdots\pi$ (**2**, **6**), C-H \cdots Cl/Br (**4**, **6**) and Cl \cdots Cl (**4**) type, which are further strengthening the crystal lattice (Table S3).

In the molecular structure of compound **5**, the terminal $-\text{C}_6\text{H}_4\text{X}$ groups of the diazenyl ligands are disposed *anti* (Figure 5), thus inducing a tubular 1D assembly based on a complex combination of $\pi\cdots\pi$, Br $\cdots\pi$, C-H \cdots O and C-H $\cdots\pi$ interactions involving the salicylate and $-\text{C}_6\text{H}_4\text{Br}$ groups of the $(\text{HL}^{\text{BASA}})^-$ ligands (Figure 11). The resulting 1D strands are oriented along [0 0 1] and interact

TABLE 2 Selected bond distances (Å) and bond angles (°) for compounds 1–6^a

	1	2	3	4	5	6
Zn–O _{OCO}	1.9488(17)	1.971(2)	1.991(2)	2.002(3)	1.971(3) / 1.957(3)	2.011(5)
Zn···O _{OCO}	2.865(2)	2.777(3)	2.688(3)	2.691(4)	2.647(4) / 2.761(4)	2.704(7)
Zn–N _{py}	2.0275(19)	2.031(2)	2.037(3)	2.048(3)	2.046(4) / 2.065(4)	2.040(5)
O _{OCO} –Zn–O _{OCO}	103.37(10)	99.76(12)	96.78(14)	96.09(16)	128.41(14)	98.5(3)
O _{OCO} ···Zn···O _{OCO}	176.43(6)	173.58(8)	177.9(1)	179.6(1)	83.4(1)	179.1(2)
O _{OCO} –Zn–N _{py}	101.09(8)	101.60(10)	101.38(11)	101.51(12)	102.08(14) / 110.76(15)	101.0(2)
	124.22(8)	124.64(10)	129.17(10)	129.35(11)	100.27(15) / 109.77(16)	128.8(2)
N _{py} –Zn–N _{py}	104.99(11)	106.69(13)	102.77(15)	102.86(15)	103.25(14)	102.5(3)

^aExcept for 5, the molecular structures exhibit crystallographic symmetry (2-axis).

**FIGURE 7** Comparison of the coordination polyhedra in compounds 1 and 5. Symmetry operator: (i) 1–x, y, 0.5–z

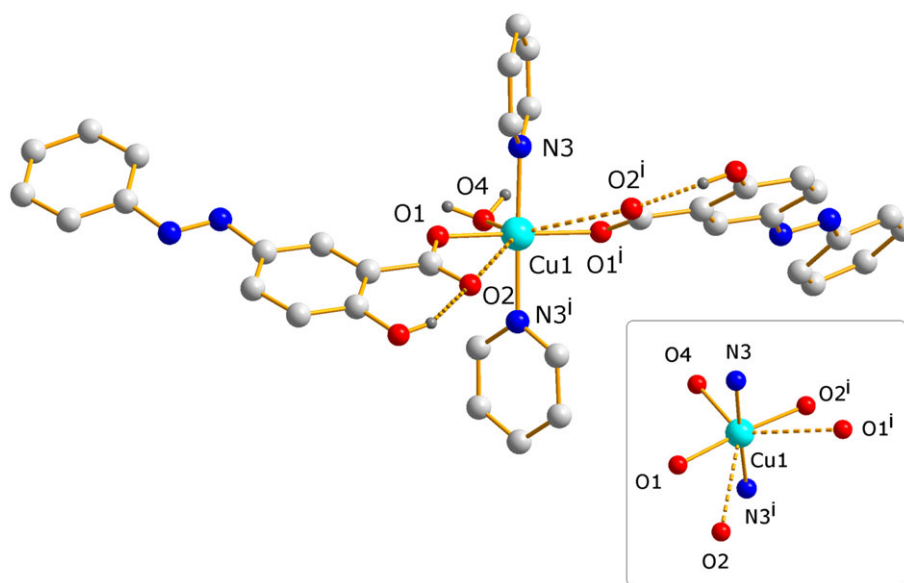
with adjacent strands through a series of C–H···O, C–H···N, C–H···π, π···π and C–H···Br contacts (Table S4).

Although the supramolecular organization of compound 5 seems to be more complex than that of

TABLE 3 Selected bond distances (Å) and bond angles (°) for compound 7^a

Cu–N _{py}	2.003(3)
Cu–O _{OCO}	1.973(3)
Cu···O _{OCO}	3.014(4)
Cu–O _w	2.214(4)
N _{py} –Cu–N _{py}	176.0(2)
O _{OCO} –Cu–O _{OCO}	174.0(2)
O _{OCO} –Cu–O _w	93.01(10)
N _{py} –Cu–O _{OCO}	89.32(13) / 90.47(13)
N _{py} –Cu–O _w	91.99(11)

^aThe molecular structure of 7 exhibits crystallographic symmetry (2-axis).

**FIGURE 8** Perspective view of the molecular structure of compound 7 with partial atom labeling scheme. Symmetry operator: (i) 1–x, 1–y, z. For clarity, most of the hydrogen atoms are omitted and disordered hydrogen atoms of the O_w is not shown

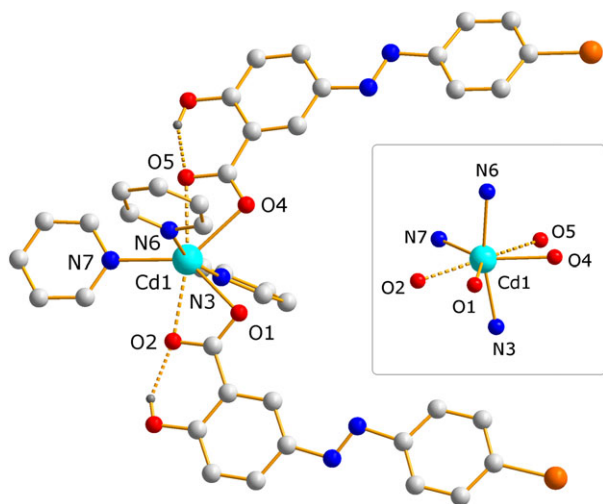


FIGURE 9 Perspective view of the molecular structure of compound **8** with partial atom labeling scheme. For clarity, most of the hydrogen atoms are omitted

TABLE 4 Bond distances (Å) and bond angles (°) for compound **8**

Cd-O1	2.406(3)	Cd-N3	2.325(4)
Cd-O2	2.464(4)	Cd-N6	2.336(4)
Cd-O4	2.349(3)	Cd-N7	2.361(4)
Cd-O5	2.560(3)		
O1-Cd-O2	53.41(11)	O2-Cd-N7	82.99(13)
O1-Cd-O4	87.31(12)	O4-Cd-N3	84.26(13)
O1-Cd-O5	140.37(11)	O4-Cd-N6	81.82(13)
O2-Cd-O4	140.59(12)	O4-Cd-N7	136.42(13)
O2-Cd-O5	164.95(11)	O5-Cd-N3	84.32(13)
O4-Cd-O5	53.24(10)	O5-Cd-N6	88.53(13)
O1-Cd-N3	88.56(13)	O5-Cd-N7	83.54(13)
O1-Cd-N6	89.32(13)	N3-Cd-N6	166.00(14)
O1-Cd-N7	136.09(13)	N3-Cd-N7	98.11(14)
O2-Cd-N3	90.97(14)	N6-Cd-N7	93.00(14)
O2-Cd-N6	98.85(13)		

complex **6**, which apart from the $(HL^{BASA})^-$ ligand carries 4-methylpyridine instead of pyridine, the melting point and, therefore, the crystal lattice energy is significantly lower (**5**, M.p. 177–178 °C; **6**, M.p. 200–202 °C). This seems to indicate that for complex **5** probably a polymorphous form exists that is isostructural with the remaining members of the Zn (II) series, which is reasonable when considering that the molecular volume of **5** is smaller when compared to compound **6** and the chlorine analogue **4** (M.p. 209–210 °C).

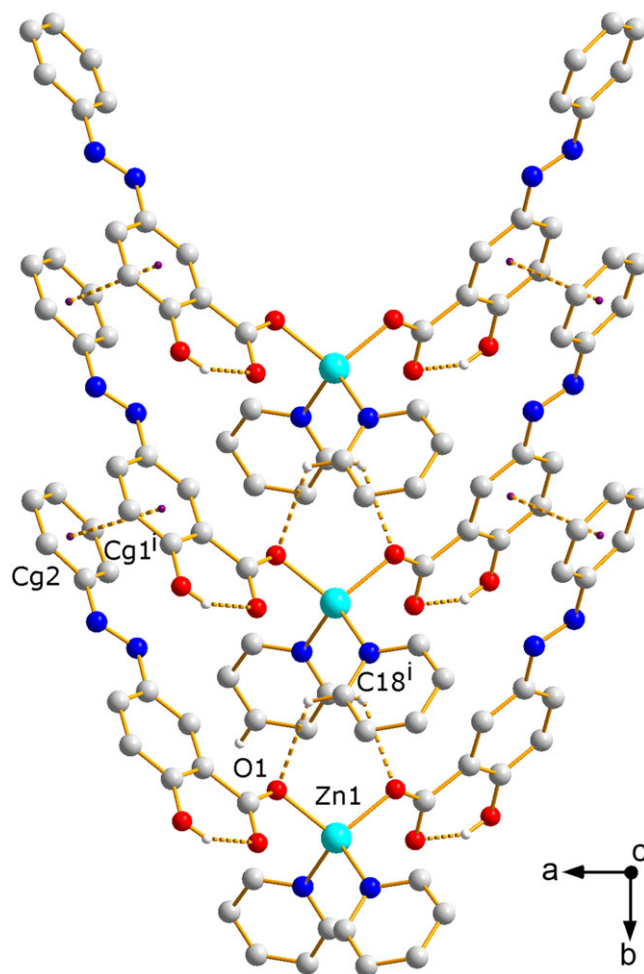


FIGURE 10 Fragment of the crystal structure of compound **1** showing the 1D strands along [0 1 0] resulting from π -stacking and C–H...O interactions. Cg1 = centroid (C2–C7); Cg2 = centroid (C8–C13). Symmetry operator: $x, -1+y, z$. For clarity, hydrogen atoms not involved in hydrogen bonding interactions are omitted

3.3.2 | Analysis of the Cu (II) and Cd (II) compounds 7–8

Metal-coordinated water molecules are excellent hydrogen bond donors, which explains the formation of 1D strands through double-bridged motifs based on $O_w-H\cdots O$ hydrogen bonds in the crystal structure of the copper complex **7**. As illustrated in Figure 12, the $(HL^{ASA})^-$ ligand molecules in the 1D strands running along [0 0 1] are further linked through π -interactions between adjacent salicylate and $-C_6H_5$ rings (centroid...centroid, 4.64 Å). In the third dimension, adjacent strands are connected only through a series of C–H... π and van der Waals contacts (Table S5).

In the Cd (II) complex **8**, the molecular units are organized by π -interactions involving the salicylate moieties of the $(HL^{ASA})^-$ ligands with centroid...centroid distances of 4.11 Å. As can be seen from Figure 13, these interactions are accomplished by C–H...O, C–H...N and C–H... π contacts

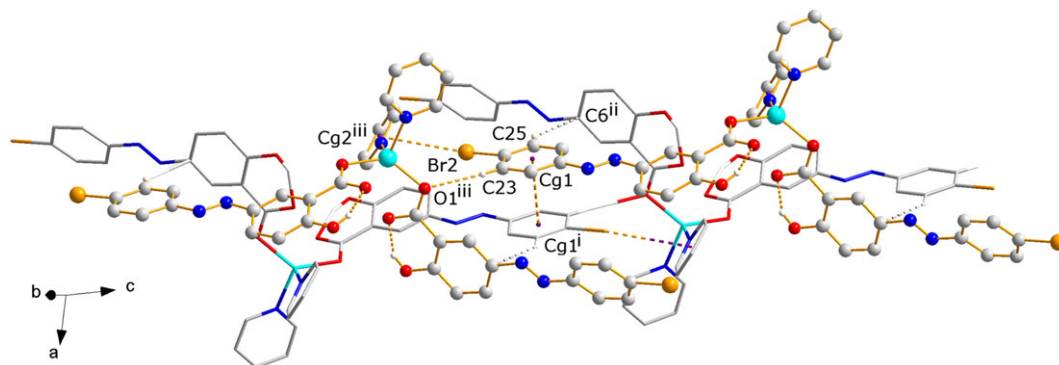


FIGURE 11 Fragment of the crystal structure of compound **5** showing the 1D strands along $[0\ 0\ 1]$ resulting from π -stacking, $\text{Br}\cdots\pi$, $\text{C}-\text{H}\cdots\text{O}$ and $\text{C}-\text{H}\cdots\pi$ interactions. Cg_5 = centroid (C21–C26). Symmetry operators: (i) $1-x, 1-y, -z$; (ii) $1-x, 1-y, 1-z$; (iii) $x, y, -1+z$. For clarity, hydrogen atoms not involved in hydrogen bonding interactions are omitted

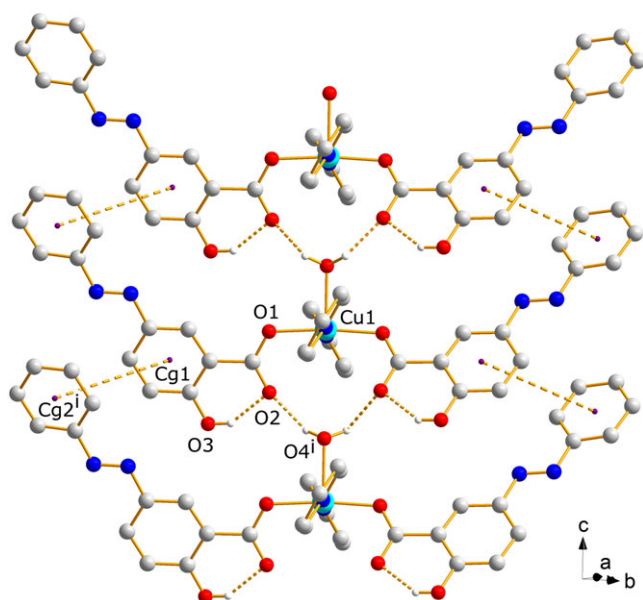


FIGURE 12 Fragment of the crystal structure of compound **7** showing the 1D strands resulting from $\text{O}_w-\text{H}\cdots\text{O}_w$ hydrogen bonds and π -stacking interactions. Cg_1 = centroid (C2–C7); Cg_2 = centroid (C8–C13). Symmetry operator: $x, y, -1 + z$. For clarity, hydrogen atoms not involved in hydrogen bonding interactions and disordered hydrogen atoms of the H_2O molecule are not shown

to give overall 2D layers. In the third dimension, besides $\text{C}-\text{H}\cdots\text{O}$ and van der Waals contacts adjacent layers are linked through two cyclic motifs involving the bromine atoms attached at the periphery of the $(\text{HL}^{\text{ASA}})^-$ ligand molecules, the first based on a $\text{C}-\text{H}\cdots\text{Br}$ and an $\text{O}\cdots\text{Br}$ contact and the second on a $\text{Br}\cdots\pi$ and a $\text{C}-\text{H}\cdots\text{N}$ interaction (Figure 14, Table S5).

3.4 | Antibacterial activity results

The solution stability of compounds **1–8** was assessed in dimethyl sulfoxide (DMSO) prior to the antibacterial

experiments. The UV/Vis absorbance spectra were monitored for two days (Figure S24; ESI[†]); the unchanged basic pattern of the spectra of the test compounds indicates that they are stable in DMSO solution.

The antibacterial potential of the pro-ligands $\text{H}_2\text{L}^{\text{XASA}}$ and the corresponding Zn (II), Cu (II) and Cd (II) compounds **1–8** along with the reference compounds ($\text{Zn}(\text{OAc})_2\cdot 2\text{H}_2\text{O}$, $\text{Cu}(\text{OAc})_2\cdot \text{H}_2\text{O}$ and $\text{Cd}(\text{OAc})_2\cdot 2\text{H}_2\text{O}$) was evaluated according to the inhibition zone formation against three bacterial strains, i.e., *Bacillus subtilis* MTCC 441, *Staphylococcus aureus* MTCC 96 and *Klebsiella pneumoniae* MTCC 109, and a fungal strain, i.e., *Candida albicans* MTCC 183. The results were compared with the activity of chloramphenicol and fluconazole as positive controls for bacteria and fungus, respectively, and the solvent used for the experiments (10% DMSO) as negative control, see Table 5 (Figures S25, S26 and S27 (Panels A–D); ESI[†]). As expected, the solvent did not inhibit the growth of the tested microorganisms.

The results of the antimicrobial screening revealed that among the twelve compounds examined ($\text{H}_2\text{L}^{\text{XASA}}$ and **1–8**), all of them could inhibit at least one of the three indicator organisms, with varying degrees of antimicrobial activity. In general, compounds **1–8** demonstrated enhanced activity against *B. subtilis* MTCC 441 when compared to their respective pro-ligands. Significant activities were noted for the zinc (II) compounds **1–3** and **6** and the cadmium (II) compound **8** against all three bacterial strains, including *K. pneumoniae* MTCC 109, which was resistant to seven of the compounds tested, including the copper (II) complex **7**. *C. albicans* MTCC 183 was susceptible to most of the compounds except for $\text{Zn}(\text{OAc})_2\cdot 2\text{H}_2\text{O}$. In general, $\text{Cd}(\text{OAc})_2\cdot 2\text{H}_2\text{O}$ was the most potent agent of all compounds, showing good activity against all test organisms.

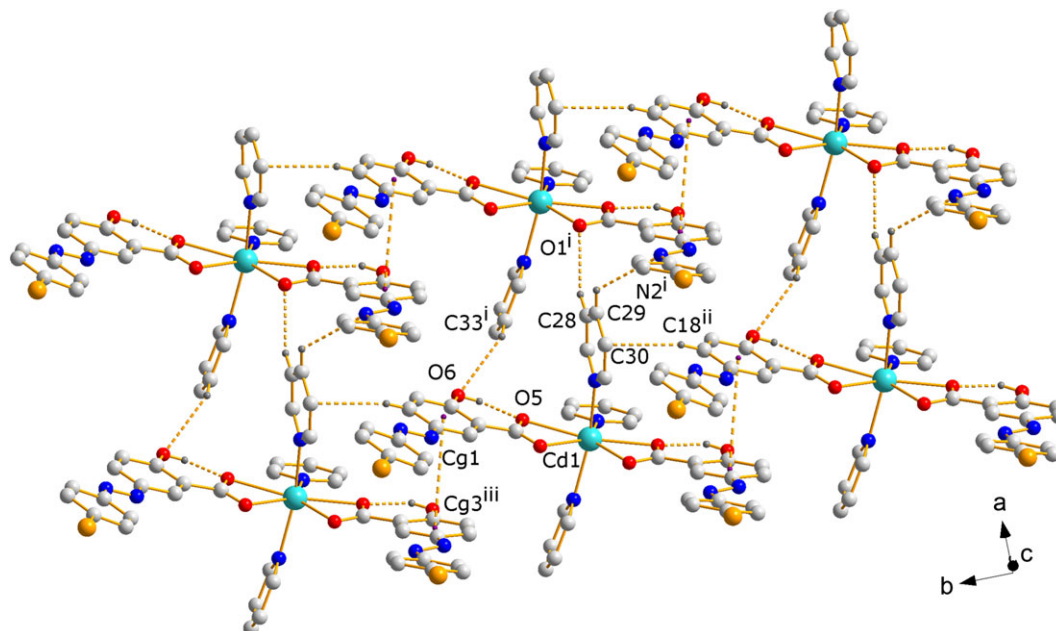


FIGURE 13 Fragment of the crystal structure of compound **8** showing the 2D layers resulting from π -stacking interactions and C–H...O, C–H...N and C–H... π contacts. Cg1 = centroid (C2–C7); Cg3 = centroid (C15–C20). Symmetry operators: (i) $1 + x, y, z$; (ii) $x, -1 + y, z$; (iii) $x, 1 + y, z$. For clarity, hydrogen atoms not involved in hydrogen bonding interactions are omitted

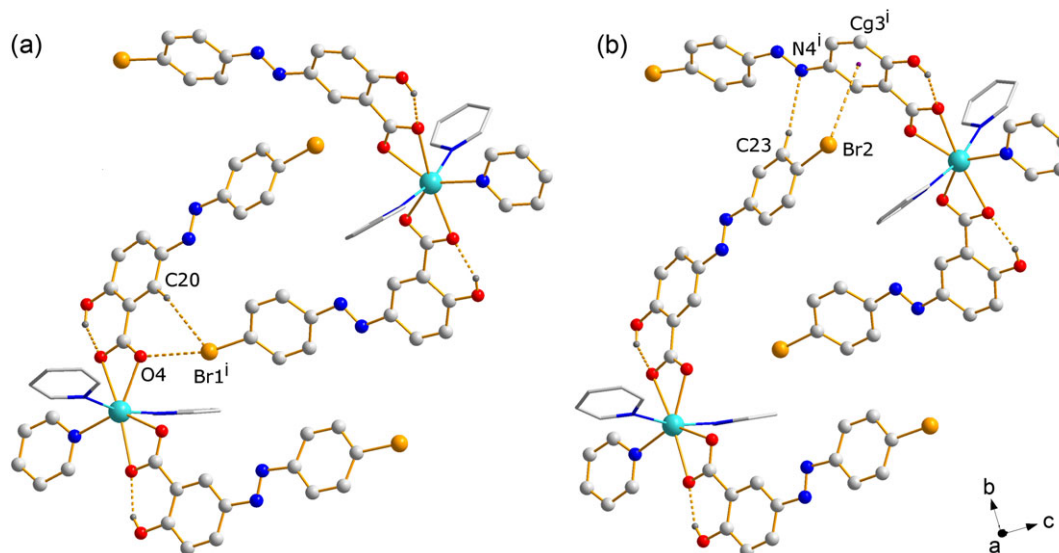


FIGURE 14 Fragments of the crystal structure of compound **8** showing the cyclic motifs based on a C–H...Br and an O...Br contact (a) and a C–H...N and Br... π contact (b). Symmetry operators: (i) $0.5-x, 0.5 + y, 1.5-z$; (ii) $1.5-x, 0.5+y, 1.5-z$. For clarity, hydrogen atoms not involved in hydrogen bonding interactions are omitted

The antimicrobial activities of the compounds studied herein are more promising than those of a recently investigated series of zinc (II) compounds with 5-[(4-(aryl)-phenyl)-1-diazenyl]quinolin-8-olates,^[20] testifying that 5-[(*E*)-2-(aryl)-1-diazenyl]-2-hydroxybenzoates are better ligands for bacterial growth inhibitors with zinc

(II). However, a more detailed interpretation of the structure–property relationships is difficult, since the microbial activities of the compounds depend on several factors such as the type and number of donor atoms, their relative positions within the ligand and the metal coordination geometry.

TABLE 5 Antimicrobial activity of the pro-ligands (H_2L^{ASA} , H_2L^{MASA} , H_2L^{CASA} and H_2L^{BASA}) and the metal compounds (**1–8**) against representative bacterial and fungal strains

Pro-ligand/Compound	Inhibition zones (in mm) observed for the tested bacterial and fungal species			
	<i>B. subtilis</i> MTCC 441	<i>S. aureus</i> MTCC 96	<i>K. pneumoniae</i> MTCC 109	<i>C. albicans</i> MTCC 183
H_2L^{ASA}	11	11	0	11
H_2L^{MASA}	19	10	0	11
H_2L^{CASA}	18	16	0	12
H_2L^{BASA}	18	11	0	12
1	21	10	10	10
2	21	10	11	13
3	26	16	10	18
4	30	24	0	21
5	31	21	0	20
6	27	19	11	22
7	18	17	0	14
8	28	23	11	22
Cu (OAc)₂·H₂O	10	0	0	14
Zn (OAc)₂·2H₂O	26	13	17	0
Cd (OAc)₂·2H₂O	40	28	16	33
Solvent (10% DMSO)	0	0	0	0
Chloramphenicol (C)³⁰	29	26	22	-
Fluconazole (FLC)²⁵	-	-	-	18

4 | CONCLUSIONS

Monomeric zinc complexes with distorted tetrahedral (**1–6**), a copper complex with a square-pyramidal (**7**) and a cadmium complex with a pentagonal-bipyramidal (**8**) coordination geometries have been obtained by using aryldiazenyl linked *O,O*-chelating (salicylates) ligands in combination with pyridine derivatives as ancillary ligands. The aryl-substituted diazosalicylate ligands are coordinated to the metal complexes only through the oxygen atoms of carboxylate groups, either in an anisobidentate or isobidentate mode. Despite the variation of the substituents at the periphery of the primary (H_2L^{XASA} ; X = H, Me, Cl, Br) and secondary ligands (4-Py-R; R = H, Me), for the Zn (II) complex series studied herein **1–6**, with one exception, the formation of isostructural solids was achieved. This illustrates that the π -electron density and energy levels can be varied without modification of the solid-state structure by changing the substituents in the aryldiazenyl salicylate ligands, thus enabling fine-tuning of its physicochemical properties. This is an important finding and fundamental for applications in electron conduction and optics. The structural analysis of the copper (II) and

cadmium (II) complexes revealed that metal ion interchange not only influences the electronic structure of the aryl-substituted diazenyl-salicylate ligand but also the solid state organization. This is due to the significant change in coordination number and geometries between these metal ions, even though they are adjacent in the periodic system of the elements.

Turning to the antimicrobial activity, compounds **1–7** and **8** were found to be more potent against *Bacillus subtilis* MTCC 441 with IZD ≥ 20 (high sensitivity) and less active against *Klebsiella pneumoniae* MTCC 109. Similar inhibitory effects were noted for the assays with *Staphylococcus aureus* MTCC 96 and *Candida albicans* MTCC 183.

ACKNOWLEDGEMENTS

Financial support from the University Grants Commission, India (Grant No. 42-396/2013 (SR) 2013, TSBB), the Council of Scientific and Industrial Research, India (Grant No. 01 (2734)/13/EMR-II, 2013, TSBB) and the University Grants Commission, India (SAP-CAS,

Phase-I) is gratefully acknowledged. KN thanks the University Grants Commission, India, for a UGC-RGNF doctoral research fellowship and IRL thanks CONACyT for a doctoral fellowship. Finally, the authors thank DST-PURSE for access to the diffractometer facility.

CONFLICT OF INTEREST

The authors declare that they have no conflicts of interest with the contents of this article.

SUPPLEMENTARY MATERIAL

Supplementary data associated with this article can be found, in the online version, at <http://XXXX>. ^1H and ^{13}C NMR spectra for **1-8** (Figures S1-S14). UV-Vis absorption spectra of the pro-ligands ($\text{H}_2\text{L}^{\text{ASA}}$, $\text{H}_2\text{L}^{\text{MASA}}$, $\text{H}_2\text{L}^{\text{CASA}}$ and $\text{H}_2\text{L}^{\text{BASA}}$) and the metal complexes **1-8** (Figure S15). Perspective views of the asymmetric units of the crystal structures of compounds **1-8** (Figures S16-S23). Stability experiments for compounds **1-8** (Figure S24). Graphic showing the zones of inhibition in the antibacterial and antifungal tests (Figures S25-S26). Comparison of the absorption maxima from the electronic spectra of pro-ligands $\text{H}_2\text{L}^{\text{XASA}}$ and compounds **1-8** (Table S1). Geometric parameters for intra- and intermolecular non-covalent interactions in the crystal structures of **1-8** (Tables S2-S5).

ORCID

Tushar S. Basu Baul  <https://orcid.org/0000-0002-9587-3503>

REFERENCES

- [1] A. Krężel, W. Maret, *Arch. Biochem. Biophys.* **2016**, *611*, 3.
- [2] a) Y. Kawakami, K. Tajima, T. Tsuruta, *Tetrahedron* **1973**, *29*, 1179; b) K. Soga, E. Imai, I. Hattori, *Polym. J. (Japan)* **1981**, *13*, 407; c) M. Super, E. Berluce, C. Costello, E. Beckman, *Macromolecules* **1997**, *30*, 368; d) D. J. Darensbourg, J. R. Wildeson, J. C. Yarbrough, *Inorg. Chem.* **2002**, *41*, 973.
- [3] a) B. List, R. A. Lerner, C. F. Barbas III., *J. Am. Chem. Soc.* **2000**, *122*, 2395; b) K. Sakthivel, W. Notz, T. Bui, C. F. Barbas III., *J. Am. Chem. Soc.* **2001**, *123*, 5260; c) A. B. Northrup, D. W. C. MacMillan, *J. Am. Chem. Soc.* **2002**, *124*, 6798; d) T. Darbre, M. Machuqueiro, *Chem. Commun.* **2003**, *15*, 1090.
- [4] a) Y. Yan, X. Lin, S. Yang, A. J. Blake, A. Dailly, N. R. Champness, P. Hubberstey, M. Schroder, *Chem. Commun.* **2009**, 1025; b) H. Deng, S. Grunder, K. E. Cordova, C. Valente, H. Furukawa, M. Hmadeh, F. Gándara, A. C. Whalley, Z. Liu, S. Asahina, H. Kazumori, M. O'Keeffe, O. Terasaki, J. F. Stoddart, O. M. Yaghi, *Science* **2012**, *336*, 1018; c) R. Nayuk, D. Zacher, R. Schweins, C. Wiktor, R. A. Fischer, G. van Tendeloo, K. Huber, *J. Phys. Chem. C* **2012**, *116*, 6127; d) P. K. Yadav, N. Kumari, P. Pachfule, R. Banerjee, L. Mishra, *Cryst. Growth Des.* **2012**, *12*, 5311; e) W. Morris, B. Volosskiy, S. Demir, F. Gándara, P. L. McGrier, H. Furukawa, D. Cascio, J. F. Stoddart, O. M. Yaghi, *Inorg. Chem.* **2012**, *51*, 6443; f) P. Lemoine, B. Viossat, G. Morgant, F. T. Greenaway, A. Tomas, N.-H. Dung, J. R. J. Sorenson, *J. Inorg. Biochem.* **2002**, *89*, 18.
- [5] M. Rizzotto, in *A Search for Antibacterial Agents*, (Ed: V. Bobbarala), InTech, Rijeka, Croatia **2012** 73.
- [6] C. R. Groom, F. H. Allen, *Angew. Chem. Int. Ed.* **2014**, *53*, 662.
- [7] P. Lemoine, A. Tomas, D. Nguyen-Huy, B. Viossat, *Z. Kristallogr. NCS* **2000**, *215*, 521.
- [8] C. Banti, A. Giannoulis, N. Kourkoumelis, A. Owczarzak, M. Kubicki, S. Hadjikakou, *J. Inorg. Biochem.* **2015**, *142*, 132.
- [9] C. F. Edwards, W. P. Griffith, A. J. White, D. J. Williams, *Polyhedron* **1992**, *11*, 2711.
- [10] N. Palanisami, G. Prabusankar, R. Murugavel, *Inorg. Chem. Commun.* **2006**, *9*, 1002.
- [11] J. A. van der Horn, B. Souvignier, M. Lutz, *Crystals* **2017**, *7*(12). <https://doi.org/10.3390/cryst7120377>
- [12] J. Sahoo, S. K. Paidesetty, *Egypt. J. Basic Appl. Sci.* **2015**, *2*, 268.
- [13] S. Jin, D. Wang, *Z. Anorg. Allg. Chem.* **2011**, *637*, 618.
- [14] R. Mishra, M. Ahmad, M. R. Tripathi, *Polyhedron* **2013**, *54*, 189.
- [15] S. Jin, H. Liu, G. Chen, Z. Y. An, Y. Lou, K. Huang, D. Wang, *Polyhedron* **2015**, *95*, 91.
- [16] H. Liu, L.-J. Song, Z.-F. Ju, W. Li, J. Zhang, *J. Mol. Struct.* **2008**, *875*, 565.
- [17] Y.-Z. Tang, Y.-H. Tan, S.-H. Chen, Y.-W. Chao, *Z. Anorg. Allg. Chem.* **2007**, *633*, 332.
- [18] P. P. Meng, L. L. Dang, X. J. Zhang, L. F. Ma, J. Q. Li, L. L. Gong, L. Zhang, L. N. Meng, F. Luo, *Cryst. Eng. Comm.* **2016**, *18*, 6336.
- [19] Y.-H. Tan, Q.-S. Li, X.-P. Luo, X.-B. Xie, *Acta Crystallogr. E* **2008**, *64*, m276.
- [20] F. Gou, X. Jiang, B. Li, H. Jing, Z. Zhu, *ACS Appl. Mater. Interfaces* **2013**, *5*, 12631.
- [21] T. S. Basu Baul, K. Nongsiej, K. Biswas, S. R. Joshi, H. Höpfl, *Inorg. Chim. Acta* **2018**, *482*, 756.
- [22] T. S. Basu Baul, S. Dhar, S. M. Pyke, E. R. T. Tiekink, E. Rivarola, R. Butcher, F. E. Smith, *J. Organomet. Chem.* **2001**, *633*, 7.
- [23] T. S. Basu Baul, S. Dhar, N. Kharbani, S. M. Pyke, R. Butcher, F. E. Smith, *Main Group Met. Chem.* **1999**, *22*, 413.
- [24] Agilent Technologies. CrysAlisPro, Version 1.171.37.35. Yarnton, Oxfordshire, United Kingdom: **2014**.
- [25] O. V. Dolomanov, L. J. Bourhis, R. J. Gildea, J. A. K. Howard, H. Puschmann, *J. Appl. Crystallogr.* **2009**, *42*, 339.
- [26] G. M. Sheldrick, *Acta Crystallogr. A* **2015**, *71*, 3.
- [27] G. M. Sheldrick, *Acta Crystallogr. C* **2015**, *71*, 3.
- [28] K. Brandenburg, *Diamond*, Version 4.3.2, Crystal Impact GbR, Bonn, Germany, **2017**.
- [29] H. D. Flack, G. Bernardinelli, *Chirality* **2008**, *20*, 681.
- [30] C. Perez, M. Paul, P. Bazerque, *Acta Bio. Med. Exp.* **1990**, *15*, 113.
- [31] G. B. Deacon, R. J. Philips, *Coord. Chem. Rev.* **1980**, *33*, 227.
- [32] K. Nakamoto, J. A. Kieft, *J. Inorg. Nucl. Chem.* **1967**, *29*, 2561.

- [33] F. T. Greenway, A. Pezeshk, A. W. Cordes, M. C. Nobel, J. R. J. Sorenson, *Inorg. Chim. Acta* **1984**, *93*, 67.
- [34] G. Davey, F. S. Stephens, *J. Chem. Soc. a* **1971**, *0*, 1917.
- [35] G. Davey, F. S. Stephens, *J. Chem. Soc. a* **1971**, *0*, 2577.
- [36] C. H. L. Kennard, E. J. O'Reilly, S. Schiller, G. Smith, A. H. White, *Aust. J. Chem.* **1986**, *39*, 1823.
- [37] G. Smith, E. J. O'Reilly, C. H. L. Kennard, T. C. W. Mak, *Inorg. Chim. Acta* **1982**, *65*, L219.
- [38] F. Valach, R. Grobelny, T. Glowiak, J. Mrozinski, V. Lukeš, Z. Blahová, *J. Coord. Chem.* **2010**, *63*, 1645.
- [39] Y.-H. Li, Y.-Z. Tang, X.-F. Huang, R.-G. Xiong, *Z. Anorg. Allg. Chem.* **2005**, *631*, 639.
- [40] J.-H. Liao, C.-D. Ho, *Acta Cryst. E* **2004**, *60*, m156.
- [41] I. F. Hernández-Ahuactzi, H. Höpfl, V. Barba, P. Román-Bravo, L. S. Zamudio-Rivera, H. I. Beltrán, *Eur. J. Inorg. Chem.* **2008**, *2008*, 2746.

SUPPORTING INFORMATION

Additional supporting information may be found online in the Supporting Information section at the end of the article.

How to cite this article: Basu Baul TS, Nongsiej K, Lamin Ka-Ot A, Joshi SR, Rojas León I, Höpfl H. Tweaking the affinity of aryl-substituted diazosalicylato- and pyridine ligands towards Zn (II) and its neighbors in the periodic system of the elements, Cu (II) and Cd (II), and their antimicrobial activity. *Appl Organometal Chem.* 2019;e4905. <https://doi.org/10.1002/aoc.4905>